Boron Cage Clusters

DOI: 10.1002/ange.201408738

Endohedral and Exohedral Metalloborospherenes: M@B_{40} (M = Ca, Sr) and M&B_{40} (M = Be, Mg)**

Hui Bai, Qiang Chen, Hua-Jin Zhai, and Si-Dian Li**

Abstract: *The recent discovery of the all-boron fullerenes or borospherenes, D_{2d} $B_{40}^{-/0}$, paves the way for borospherene chemistry. Here we report a density functional theory study on the viability of metalloborospherenes: endohedral M@B_{40} (M = Ca, Sr) and exohedral M&B_{40} (M = Be, Mg). Extensive global structural searches indicate that Ca@B_{40} (**1**, C_{2v}, $^1A_1$) and Sr@B_{40} (**3**, D_{2d}, $^1A_1$) possess almost perfect endohedral borospherene structures with a metal atom at the center, while Be&B_{40} (**5**, C_s, $^1A'$) and Mg&B_{40} (**7**, C_s, $^1A'$) favor exohedral borospherene geometries with a η^7-M atom face-capping a heptagon on the waist. Metalloborospherenes provide indirect evidence for the robustness of the borospherene structural motif. The metalloborospherenes are characterized as charge-transfer complexes ($M^{2+}B_{40}^{2-}$), where an alkaline earth metal atom donates two electrons to the B_{40} cage. The high stability of endohedral Ca@B_{40} (**1**) and Sr@B_{40} (**3**) is due to the match in size between the host cage and the dopant. Bonding analyses indicate that all 122 valence electrons in the systems are delocalized as σ or π bonds, being distributed evenly on the cage surface, akin to the D_{2d} B_{40} borospherene.*

The discovery of C_{60} buckyball was followed immediately by the synthesis of endohedral metallofullerene La@C_{60},[1] in which a lanthanum atom is encapsulated inside C_{60}. Various endohedral metallofullerenes and non-metal-doped fullerenes were subsequently reported,[1–9] including the calcium–C_{60} complex, C_{5v} Ca@C_{60},[5] which remarkably enriches the fullerene chemistry. Neighboring carbon in the periodic table, elemental boron clusters, $B_n^{-/0}$, were confirmed to possess unique planar (2D) or quasi-planar structures in a wide range of sizes (n = 3–25, 30, 35, 36) in a series of joint gas-phase photoelectron spectroscopy (PES) and first-principles investigations over the past decade.[10–17] Very recently, Zhai and co-workers reported the first all-boron fullerenes, or borospherenes: D_{2d} $B_{40}^{-/0}$.[18] This observation suggests that the 2D–3D structural transition in $B_n^{-/0}$ clusters occurs at an unprecedented size of around n = 40 and marks the genesis of borospherene chemistry, which is anticipated to closely parallel that of carbon fullerenes. With exactly half the size of the theoretically proposed cage-like B_{80} cluster, which turns out to be much less stable than its core–shell rivals,[19–26] the experimentally confirmed B_{40}^- and B_{40} borospherenes are composed of interwoven boron double chains, with two B_6 hexagons at the top and bottom and four B_7 heptagons on the waist. As the global minimum being well-separated from other low-lying isomers, the D_{2d} B_{40} neutral is 3D aromatic in nature with σ plus π double delocalization. The diameter of B_{40} borospherene is 6.2 Å, about 1.0 and 2.0 Å smaller than those of C_{60} (7.1 Å) and B_{80} (8.2 Å), respectively, which makes B_{40} a suitable candidate to accommodate a range of metal atoms or small molecules inside to form endohedral M@B_{40} borospherenes, similar to the endohedral M@C_{60}[1–5,27] and M@B_{80} species.[24–26] In the meantime, the hexagonal holes, and in particular the heptagonal holes, on the cage surface of B_{40} suggest the possibility to coordinate metal atoms in an exohedral manner. Such endohedral and exohedral complexes are intriguing from both fundamental and applied points of view.

Here we report a systematic computational study on a series of endohedral M@B_{40} and exohedral M&B_{40} metalloborospherenes (M = Be, Mg, Ca, Sr) at the density functional theory (DFT) level, which aims to explore the potential of the B_{40} borospherene as a molecular device. Extensive structural searches indicate that both Ca@B_{40} (**1**, C_{2v}, $^1A_1$) and Sr@B_{40} (**3**, D_{2d}, $^1A_1$) possess endohedral structures as their global minima with the metal atom residing inside the cage, whereas Be&B_{40} (**5**, C_s, $^1A'$) and Mg&B_{40} (**7**, C_s, ^1A) adopt exohedral geometries with a η^7 face-capping metal atom. The metalloborospherenes turn out to be charge-transfer complexes between M^{2+} and B_{40}^{2-}, which maintain the structural and chemical integrity of the B_{40} cage, featuring σ plus π double delocalization in chemical bonding, akin to the D_{2d} B_{40} borospherene. This work suggests the viability of the MB_{40} metalloborospherenes and represents the simplest chemistry of borospherenes.

We start with and mainly focus on the endohedral C_{2v} Ca@B_{40} (**1**) metalloborospherene, whose C_{60}-based analogue, C_{5v} Ca@C_{60}, is experimentally known.[5] Global structural searches for CaB_{40} were performed using the Minima Hopping (MH) algorithm; see the Methods Section for details.[21,28,29] Over 3500 stationary points on the potential energy surface were probed from seven independent MH runs with different initial structures. Extensive manual structural

[*] H. Bai, Q. Chen, Prof. Dr. H. J. Zhai, Prof. Dr. S. D. Li
Nanocluster Laboratory, Institute of Molecular Science
Shanxi University, Taiyuan 030006 (China)
E-mail: hj.zhai@sxu.edu.cn
lisidian@sxu.edu.cn
Prof. Dr. H. J. Zhai
State Key Laboratory of Quantum Optics and Quantum Optics Devices, Shanxi University, Taiyuan 030006 (China)

[**] This work was supported by the National Natural Science Foundation of China (21243004, 21373130), the Shanxi International Cooperation Project (201308018), and the State Key Laboratory of Quantum Optics and Quantum Optics Devices (KF201402). H.J.Z. gratefully acknowledges the start-up fund from Shanxi University for support.

Supporting information for this article is available on the WWW under http://dx.doi.org/10.1002/anie.201408738.

 © 2015 Wiley-VCH Verlag GmbH & Co. KGaA, Weinheim

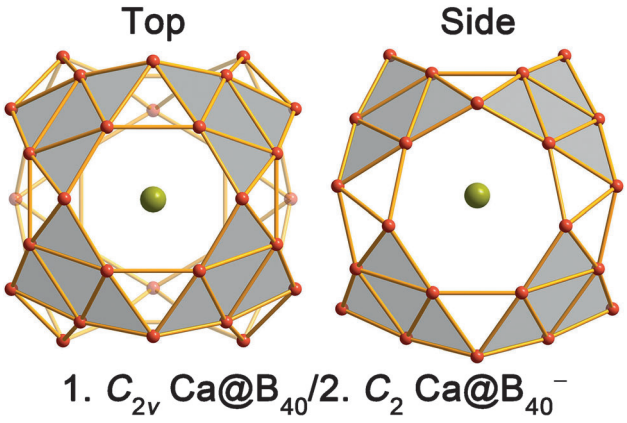

Figure 1. Optimized structures of C_{2v} Ca@B_{40} (**1**) and C_2 Ca@B_{40}^- (**2**) at the PBE0/6-311+G* level. The structural difference between the neutral and the anion is minor, and only the neutral structure is depicted. Left: top view. Right: side view.

constructions were also performed, based on the low-lying isomers of B_{40}.[18] Figure 1 displays the top and side views of C_{2v} Ca@B_{40} ($^1A_1$) (**1**) and its slightly distorted monoanion C_2 Ca@B_{40}^- (^2A) (**2**), which were optimized at the hybrid DFT–PBE0 level.[30] Alternative low-lying isomers of CaB_{40} are shown in Figure S1 in the Supporting Information. Interestingly and encouragingly, the manually constructed endohedral C_{2v} Ca@B_{40} (**1**) turns out to be the well-defined global minimum, with the alternative structures being at least 0.5 eV higher in energy at PBE0 level. The Ca atom in Ca@B_{40} (**1**) is slightly off the molecular center by 0.27 Å, along the C_2 molecular axis. For comparison, in C_{5v} Ca@C_{60}, Ca is 0.70 Å off the cage center along the C_5 axis.[5] The perfect D_{2d} Ca@B_{40} endohedral structure lies only 0.02 eV above C_{2v} Ca@B_{40} (**1**), and the former proves to be a transition state with an imaginary frequency of 80 cm^{-1} (b_2) leading to the latter. Thus, Ca@B_{40} possesses practically two equivalent C_{2v} global minimum structures, which are interconvertible via the shuffling of the Ca center atom along the C_2 axis through the D_{2d} transition state, almost barrierlessly.

We note that the second, third, and the seventh lowest-lying isomers of CaB_{40} are also endohedral metalloborospherenes (Figure S1 a), and the exohedral C_s Ca&B_{40} lies much higher above the global minimum by 1.23 eV at PBE0. All other low-lying isomers in between adopt triple-ring tubular structures with a metal atom inside the tube. The calculated relative energies for the top ten isomers at the DFT-TPSSh level[31] generally agree with those obtained at the PBE0 level (Figure S1 a). The concerted PBE0 and TPSSh data lend considerable credence that C_{2v} (**1**) is the lowest-lying isomer of the system.

Molecular dynamics (MD) simulations[32] were performed to show the dynamic stability of the endohedral C_{2v} Ca@B_{40} (**1**), as summarized in Figure S2. Its structural integrity is well preserved during MD simulations for 30 ps at both 300 and 700 K, with the root-mean-square-deviation (RMSD) of 0.11 and 0.14 Å, respectively, and maximum bond length deviation (MAXD) of 0.43 and 0.55 Å (on average) with respect to the global minimum. The B_{40} cage serves as a robust structural unit in the dynamic processes, with the metal center being well confined inside the cage in concerted mechanisms.

To shed further light on the stability of the endohedral metalloborospherene C_{2v} Ca@B_{40} (**1**), we analyzed its chemical bonding via the adaptive natural density partitioning (AdNDP) analyses,[33] which is an extension of the natural bond orbital (NBO) analyses. As shown in Figure 2, AdNDP reveals forty 3c–2e σ bonds on the 40 B_3 triangles and eight 6c–2e σ bonds on 8 quasi-planar close-packed B_6 triangles on the B_{40} cage surface. As the central B_3 triangles make major contributions to the 6c–2e σ bonds, all 48 σ bonds mentioned above can be practically viewed as delocalized 3c–2e σ bonds, one σ bond for every B_3 triangle. The remaining 13 bonds form the π framework, which are readily classified into four sets: four 5c–2e π bonds and four 7c–2e π bonds at the top and bottom of the cage, four 6c–2e π bonds on the waist, and one 40c–2e π bond over the entire cage surface. Overall, the 13 delocalized π bonds again cover the whole cage surface almost evenly. Therefore, there exists a double (σ plus π) delocalization of the electron clouds along the interwoven double chains on the molecular surface, rendering high stability to the system despite its intrinsic electron deficiency. Such a bonding pattern is very similar to that of D_{2d} B_{40} borospherene,[18] except for an additional 40c–2e π bond in Ca@B_{40} (**1**), which corresponds to the LUMO (b_2) of D_{2d} B_{40}. As will be discussed below, Ca@B_{40} (**1**) is essentially a charge-transfer complex between Ca^{2+} and B_{40}^{2-}. Apparently, the introduction of a Ca^{2+} counterion into the D_{2d} B_{40}^{2-} dianion effectively stabilizes the system (Figure S3). The close similarity between C_{2v} Ca@B_{40} (**1**) and D_{2d} B_{40} in terms of the bonding pattern further demonstrates the chemical robustness of the D_{2d} B_{40} borospherene.

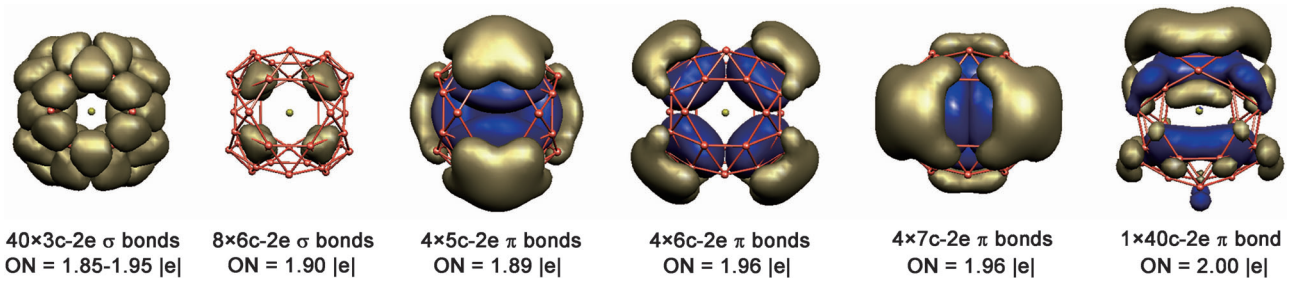

Figure 2. Bonding pattern of C_{2v} Ca@B_{40} (**1**) from adaptive natural density partitioning (AdNDP) analyses. The occupation numbers (ONs) are indicated.

© 2015 Wiley-VCH Verlag GmbH & Co. KGaA, Weinheim

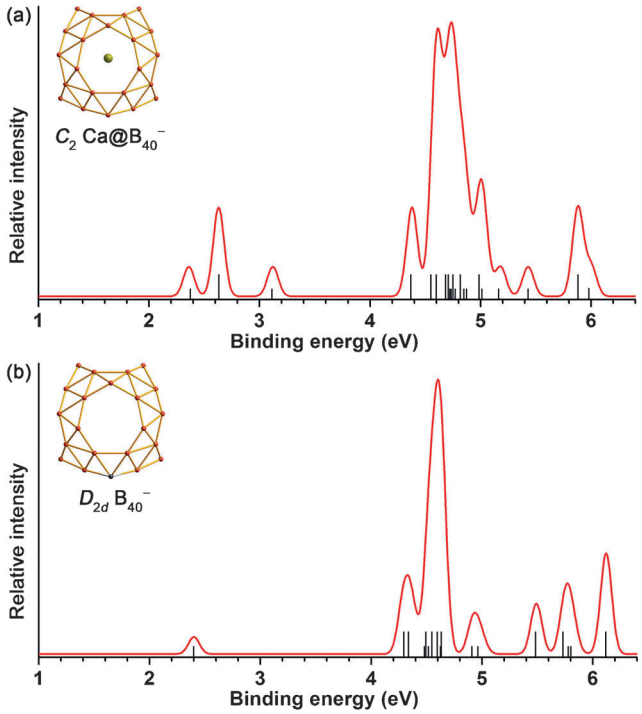

Figure 3. Simulated photoelectron spectrum of a) C_2 Ca@B_{40}^- (**1**), as compared with that of b) D_{2d} B_{40}^-.

To facilitate future experimental characterization of the C_{2v} Ca@B_{40} (**1**) endohedral metalloborospherene, we simulate the PES spectrum of its C_2 Ca@B_{40}^- (**2**) monoanion (Figure 3) using the time-dependent DFT (TD-DFT) approach.[34] The simulated PES spectrum of C_2 Ca@B_{40}^- appears similar to the experimentally observed spectrum of D_{2d} B_{40}^-,[18] except for the first three weak peaks. C_2 Ca@B_{40}^- is predicted to have an extremely low first vertical detachment energy (VDE) at 2.35 eV (^{1}A), which is even lower than that of D_{2d} B_{40}^- (experimental first VDE: 2.65 eV). This weak band of C_2 Ca@B_{40}^- originates from the detachment of the electron from the singly occupied molecular orbital (α-SOMO), which is not occupied in D_{2d} B_{40}^- (Figure S3). The second calculated VDE of C_2 Ca@B_{40}^- at 2.62 eV (^{3}B) originates from detaching the electron from β-HOMO−1, whereas the third weak VDE at 3.11 eV (^{1}B) comes from the electron detachment from α-HOMO−1. The sizable energy gap of C_2 Ca@B_{40}^- in the 3.1–4.4 eV regime is a roughly reflection of the energy gap in D_{2d} B_{40}^-, which measures the electronic robustness of the D_{2d} B_{40} borospherene. Higher excited states of D_{2d} B_{40}^- are also inherited in the simulated PES spectrum of C_2 Ca@B_{40}^-, although they may have different energy orders.

Given the fact that Be, Mg, Ca, and Sr are in the same group in the periodical table, comparative structural searches and DFT calculations are also performed for other alkaline earth metal–B_{40} complexes, based on the results obtained for CaB_{40} and CaB_{40}^-. Figure 4 displays the top and side views of D_{2d} Sr@B_{40} (^{1}A_1) (**3**), C_s Be&B_{40} (^{1}A′) (**5**), and C_s Mg&B_{40} (^{1}A′) (**7**) and their monoanions C_2 Sr@B_{40}^- (^{2}A) (**4**), C_s Be&B_{40}^- (^{2}A′) (**6**), and C_s Mg&B_{40}^- (^{2}A′) (**8**) at DFT-PBE0 level.[30] Typical low-lying isomers of SrB_{40}, BeB_{40}, and MgB_{40} are collected in Figure S1. The endohedral Sr@B_{40} (**3**) with perfect D_{2d} symmetry turns out to be the well-defined global minimum of the system, being at least 0.40 eV lower than alternative isomers. This observation suggests that the Sr center atom is an ideal match for the B_{40} cage geometrically in the endohedral configuration. Note that the exohedral C_s Sr&B_{40} is found to be much less stable (by 1.49 eV). Not surprisingly, the MD simulations (Figure S2) suggest that Sr@B_{40} (**3**) is dynamically even more robust than Ca@B_{40} (**1**), with smaller RMSD and MAXD values for the former complex.

In contrast to Ca and Sr, the Be and Mg dopants with smaller atomic radii favor the exohedral C_s Be&B_{40} (^{1}A′) (**5**) and C_s Mg&B_{40} (^{1}A′) (**7**) over their endohedral counterparts, with C_{2v} Be@B_{40} and C_{2v} Mg@B_{40} being 3.24 and 0.88 eV higher in energy, respectively, at the PBE0 level. In the exohedral metalloborospherenes, the Be and Mg dopants occupy a B_7 heptagon on the waist in a face-capping η^7 configuration. The primary reason is that the small sizes of Be and Mg mismatch the B_{40} cage in the endohedral configuration. In the exohedral structures, Be fits a B_7 heptagon best to form an almost perfect hepta-coordinated metal center, while Mg forms a convex structure with large strain due to size effect (Figure 4). Thus, with decreasing atomic radii from Sr (2.15 Å), Ca (1.97 Å), Mg (1.60 Å), to Be (1.13 Å), the alkaline earth metals move from inside to outside of the B_{40} cage, with Sr residing exactly at the cage

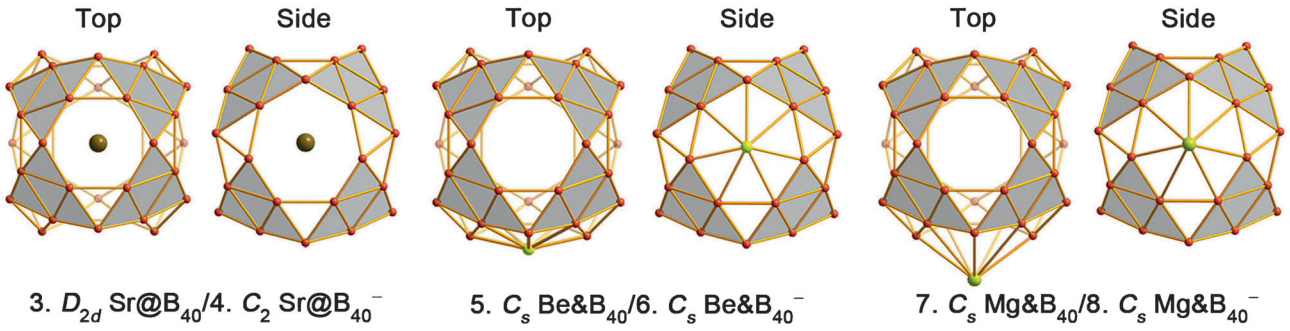

Figure 4. Top and side views of the optimized structures of D_{2d} Sr@B_{40} (^{1}A_1) (**3**), C_s Be&B_{40} (^{1}A′) (**5**), and C_s Mg&B_{40} (^{1}A′) (**7**) at the PBE0/6-311+G* level, along with their monoanions C_2 Sr@B_{40}^- (^{2}A) (**4**), C_s Be&B_{40}^- (^{2}A′) (**6**), and C_s Mg&B_{40}^- (^{2}A′) (**8**). The structural difference between the neutral and its corresponding anion is minor, and only the neutral structure is depicted.

© 2015 Wiley-VCH Verlag GmbH & Co. KGaA, Weinheim

center and Be forming an almost perfectly filled heptagon on the cage surface.

The C_{2v} Ca@B_{40} (**1**), D_{2d} Sr@B_{40} (**3**), C_s Be&B_{40} (**5**), and C_s Mg&B_{40} (**7**) series have the negative formation energies of −82.2, −78.5, −20.0, and −67.1 kcal mol^{-1}, respectively, at the PBE0 level with respect to $M + B_{40} = MB_{40}$, suggesting substantial interactions between M and B_{40}. Note that Mg possesses the lowest formation energy, which is mainly due to size effect: Mg stays the farthest from the center of the B_{40} cage (Figure 4). The calculated natural atomic charges are +1.57 |e| for Be, +1.18 |e| for Mg, +1.60 |e| for Ca, and +1.58 |e| for Sr, indicating that alkaline earth metals in the metalloborospherenes serve as donors for two electrons to the B_{40} cage, forming typical charge-transfer $M^{2+}B_{40}^{2-}$ complexes. Furthermore, the high stability of C_{2v} Ca@B_{40} (**1**) and D_{2d} Sr@B_{40} (**3**) may also be related to the weak back-donation from the negatively charged B_{40} cage to the empty d levels of Ca and Sr.[35] Indeed, the electronic configurations of the metal centers are Ca [Ar]$4s^{0.21}3d^{0.15}$ in **1** and Sr [Kr]$5s^{0.16}4d^{0.20}$ in **3**. Such coordination interaction does not exist in BeB_{40} and MgB_{40}.

As collectively shown in Figure S4, the simulated PES spectra of the whole series of C_2 Ca@B_{40}^- (**2**), C_2 Sr@B_{40}^- (**4**), C_s Be&B_{40}^- (**6**), and C_s Mg&B_{40}^- (**8**) are similar to and closely related with that of D_{2d} B_{40}^-, despite their differences in geometries. The calculated infrared (IR) absorption spectra of C_{2v} Ca@B_{40} (**1**) and D_{2d} Sr@B_{40} (**2**) neutrals as depicted in Figure S5 also exhibit the main vibrational features of the D_{2d} B_{40} cage, with three characteristic vibrational peaks at 1274(e), 821(e), and 380(e) cm^{-1}, respectively, well supporting the notion of structural, chemical, and spectroscopic integrity of the D_{2d} B_{40} cage. The predicted spectroscopic data should aid the forthcoming experimental characterizations of the endohedral and exohedral metalloborospherenes. Lastly, the predicted vertical ionization potentials of C_s Be&B_{40} (**5**), C_s Mg&B_{40} (**7**), C_{2v} Ca@B_{40} (**1**), and D_{2d} Sr@B_{40} (**3**) are 6.01, 5.94, 5.94, and 5.90 eV at the PBE0 level, respectively, which differ markedly from that of D_{2d} B_{40} (7.49 eV at the same level), suggesting opportunities to tune the electronic properties of borospherenes via doping.

In conclusion, we have explored the viability of endohedral M@B_{40} (M = Ca, Sr) and exohedral M&B_{40} (M = Be, Mg) metalloborospherenes, via global structural searches, electronic structure calculations, and chemical bonding analyses. The computational data demonstrated the structural, chemical, and spectroscopic robustness of the B_{40} borospherene, which has been experimentally observed lately. The atomic radius of the M dopant appears to be critical in stabilizing the endohedral versus exohedral configurations of metalloborospherenes. All these metalloborospherenes are charge-transfer $M^{2+}B_{40}^{2-}$ complexes. The current results provide valuable information for potential applications of the $B_{40}^{-/0}$ borospherenes as a molecular device, analogous to C_{60}.

Methods Section

Global-minimum structural searches were carried out for CaB_{40} using the Minima Hopping (MH) algorithm,[21,28,29] with the aid of extensive manual structural constructions as well. Seven independent MH runs were conducted from different initial structures, based on the low-lying isomers of $B_{40}^{0/-}$ clusters reported in literature.[18] A total of 3500 stationary points on the potential surface were probed. Subsequently, the low-lying isomers were fully optimized at the PBE0/6-311 + G* level,[30,36] which has been benchmarked in prior works as a reliable method for boron clusters, in particular in terms of energetics.[22,37] For comparison, the TPSSh/6-311 + G*[31] energies were calculated for the low-lying isomers within 1.0 eV above the global minimum at PBE0/6-311 + G*. All the energies were corrected for zero-point energies. The corresponding low-lying isomers of MB_{40} (M = Sr, Be, Mg) were also optimized at PBE0/6-311 + G* level (the Stuttgart relativistic small-core pseudopotential and valence basis set was used[38,39] for Sr). Frequency calculations were done to confirm that the reported structures are true minima. Natural atomic charges were obtained by the natural bond orbital (NBO) analyses.[40] The simulated photoelectron spectra were calculated using time-dependent DFT (TD-DFT).[34] Chemical bonding were elucidated via the adaptive natural density partitioning (AdNDP) analyses.[33] Molecular dynamics simulations were conducted using the software suite CP2K.[32] All electronic structure calculations were performed using Gaussian 09 package.[41]

Received: September 2, 2014
Published online: November 21, 2014

Keywords: alloy boron clusters · borospherenes · density functional theory · electron delocalization · metalloborospherenes

[1] J. R. Heath, S. C. O'Brien, Q. Zhang, Y. Liu, R. F. Curl, H. W. Kroto, F. K. Tittel, R. E. Smalley, *J. Am. Chem. Soc.* **1985**, *107*, 7779 – 7780.
[2] Z. Wan, J. F. Christian, S. L. Anderson, *Phys. Rev. Lett.* **1992**, *69*, 1352 – 1355.
[3] P. Weis, R. D. Beck, G. Bräuchle, M. M. Kappes, *J. Chem. Phys.* **1994**, *100*, 5684 – 5695.
[4] Y. Kubozono, H. Maeda, Y. Takabayashi, K. Hiraoka, T. Nakai, S. Kashino, S. Emura, S. Ukita, T. Sogabe, *J. Am. Chem. Soc.* **1996**, *118*, 6998 – 6999.
[5] L. S. Wang, J. M. Alford, Y. Chai, M. Diener, J. Zhang, S. M. McClure, T. Guo, G. E. Scuseria, R. E. Smalley, *Chem. Phys. Lett.* **1993**, *207*, 354 – 359.
[6] M. Saunders, R. J. Cross, H. A. Jiménez-Vázquez, R. Shimshi, A. Khong, *Science* **1996**, *271*, 1693 – 1697.
[7] T. A. Murphy, T. Pawlik, A. Weidinger, M. Höhne, R. Alcala, J. M. Spaeth, *Phys. Rev. Lett.* **1996**, *77*, 1075 – 1078.
[8] J. Lu, X. W. Zhang, X. G. Zhao, *Chem. Phys. Lett.* **1999**, *312*, 85 – 90.
[9] M. Waiblinger, K. Lips, W. Harneit, A. Weidinger, E. Dietel, A. Hirsch, *Phys. Rev. B* **2001**, *63*, 045421.
[10] H. J. Zhai, A. N. Alexandrova, K. A. Birch, A. I. Boldyrev, L. S. Wang, *Angew. Chem. Int. Ed.* **2003**, *42*, 6004 – 6008; *Angew. Chem.* **2003**, *115*, 6186 – 6190.
[11] H. J. Zhai, B. Kiran, J. Li, L. S. Wang, *Nat. Mater.* **2003**, *2*, 827 – 833.
[12] B. Kiran, S. Bulusu, H. J. Zhai, S. Yoo, X. C. Zeng, L. S. Wang, *Proc. Natl. Acad. Sci. USA* **2005**, *102*, 961 – 964.
[13] W. Huang, A. P. Sergeeva, H. J. Zhai, B. B. Averkiev, L. S. Wang, A. I. Boldyrev, *Nat. Chem.* **2010**, *2*, 202 – 206.
[14] E. Oger, N. R. Crawford, R. Kelting, P. Weis, M. M. Kappes, R. Ahlrichs, *Angew. Chem. Int. Ed.* **2007**, *46*, 8503 – 8506; *Angew. Chem.* **2007**, *119*, 8656 – 8659.
[15] W. L. Li, Y. F. Zhao, H. S. Hu, J. Li, L. S. Wang, *Angew. Chem. Int. Ed.* **2014**, *53*, 5540 – 5545; *Angew. Chem.* **2014**, *126*, 5646 – 5651.

 © 2015 Wiley-VCH Verlag GmbH & Co. KGaA, Weinheim

[16] W. L. Li, Q. Chen, W. J. Tian, H. Bai, Y. F. Zhao, H. S. Hu, J. Li, H. J. Zhai, S. D. Li, L. S. Wang, *J. Am. Chem. Soc.* **2014**, *136*, 12257 – 12260.
[17] Z. A. Piazza, H. S. Hu, W. L. Li, Y. F. Zhao, J. Li, L. S. Wang, *Nat. Commun.* **2014**, *5*, 3113.
[18] H. J. Zhai, Y. F. Zhao, W. L. Li, Q. Chen, H. Bai, H. S. Hu, Z. A. Piazza, W. J. Tian, H. G. Lu, Y. B. Wu, Y. W. Mu, G. F. Wei, Z. P. Liu, J. Li, S. D. Li, L. S. Wang, *Nat. Chem.* **2014**, *6*, 727 – 731.
[19] N. G. Szwacki, A. Sadrzadeh, B. Yakobson, *Phys. Rev. Lett.* **2007**, *98*, 166804.
[20] D. L. V. K. Prasad, E. D. Jemmis, *Phys. Rev. Lett.* **2008**, *100*, 165504.
[21] S. De, A. Willand, M. Amsler, P. Pochet, L. Genovese, S. Goedecker, *Phys. Rev. Lett.* **2011**, *106*, 225502.
[22] F. Y. Li, P. Jin, D. Jiang, L. Wang, S. B. Zhang, J. Zhao, Z. Chen, *J. Chem. Phys.* **2012**, *136*, 074302.
[23] P. Boulanger, M. Morinière, L. Genovese, P. Pochet, *J. Chem. Phys.* **2013**, *138*, 184302.
[24] P. Jin, C. Hao, Z. X. Gao, S. B. Zhang, Z. F. Chen, *J. Phys. Chem. A* **2009**, *113*, 11613 – 11618.
[25] J. L. Li, G. W. Yang, *J. Phys. Chem. C* **2009**, *113*, 18292 – 18295.
[26] J. T. Wang, C. F. Chen, E. G. Wang, D. S. Wang, H. Mizuseki, Y. Kawazoe, *Appl. Phys. Lett.* **2009**, *94*, 133102.
[27] C. Thilgen, *Angew. Chem. Int. Ed.* **2012**, *51*, 587 – 589; *Angew. Chem.* **2012**, *124*, 607 – 609.
[28] S. Goedecker, *J. Chem. Phys.* **2004**, *120*, 9911 – 9917.
[29] S. Goedecker, W. Hellmann, T. Lenosky, *Phys. Rev. Lett.* **2005**, *95*, 055501.
[30] C. Adamo, V. Barone, *J. Chem. Phys.* **1999**, *110*, 6158 – 6170.
[31] J. Tao, J. P. Perdew, V. N. Staroverov, G. E. Scuseria, *Phys. Rev. Lett.* **2003**, *91*, 146401.
[32] J. VandeVondele, M. Krack, F. Mohamed, M. Parrinello, T. Chassaing, J. Hutter, *Comput. Phys. Commun.* **2005**, *167*, 103 – 128.
[33] D. Y. Zubarev, A. I. Boldyrev, *Phys. Chem. Chem. Phys.* **2008**, *10*, 5207 – 5217.
[34] R. Bauernschmitt, R. Ahlrichs, *Chem. Phys. Lett.* **1996**, *256*, 454 – 464.
[35] M. Yoon, S. Yang, C. Hicke, E. Wang, D. Geohegan, Z. Zhang, *Phys. Rev. Lett.* **2008**, *100*, 206806.
[36] R. Krishnan, J. S. Binkley, R. Seeger, J. A. Pople, *J. Chem. Phys.* **1980**, *72*, 650 – 654.
[37] H. Bai, Q. Chen, C. Q. Miao, Y. W. Mu, Y. B. Wu, H. G. Lu, H. J. Zhai, S. D. Li, *Phys. Chem. Chem. Phys.* **2013**, *15*, 18872 – 18880.
[38] D. Feller, *J. Comput. Chem.* **1996**, *17*, 1571 – 1586.
[39] K. L. Schuchardt, B. T. Didier, T. Elsethagen, L. Sun, V. Gurumoorthi, J. Chase, J. Li, T. L. Windus, *J. Chem. Inf. Model.* **2007**, *47*, 1045 – 1052.
[40] E. D. Glendening, J. K. Badenhoop, A. E. Reed, J. E. Carpenter, J. A. Bohmann, C. M. Morales, F. Weinhold, NBO 5.0., Theoretical Chemistry Institute, University of Wisconsin, Madison, **2001**.
[41] Gaussian 09 (Revision A.2), M. J. Frisch, et al., Gaussian Inc., Wallingford, Connecticut, **2009**.

 © 2015 Wiley-VCH Verlag GmbH & Co. KGaA, Weinheim